Characterization of stilbene and EJ-276 scintillators coupled with a large area SiPM array for a fast neutron dose rate detector

F. Ferrulli, N. Dinar, L. Gallego Manzano, M. Labalme, M. Silari

Version of Record: https://www.sciencedirect.com/science/article/pii/S0168900221005519
Manuscript_f9f9a20b5a5ddace95bd6498e50271c0

Characterisation of stilbene and EJ-276 scintillators coupled with a large area SiPM array for a fast neutron dose rate detector.

F. Ferrulli[1,2,*], N. Dinar[2], L. Gallego Manzano[2,3], M. Lablme[1], M. Silari[2]

[1]Université de CAEN, CAEN, France

[2]CERN, 1211 Geneve 23, Switzerland

[3]Now at the Institute of Radiation Physics, Lausanne University Hospital and Lausanne University, Switzerland

Abstract—A 1-inch stilbene and EJ-276 (plastic) organic scintillators were characterised in view of their use in a portable survey meter for fast neutron detection and dose rate measurements in radiation protection. They were coupled with a large area Silicon Photomultiplier (SiPM) array and characterised in terms of neutron/γ–ray (n/γ) discrimination capability, count rate linearity, count rate saturation effects, temperature stability and neutron detection efficiency. A Pile-Up Rejection (PUR) algorithm was developed and tested to increase their count rate linearity with increasing dose rate. Results show that the stilbene exhibits better performance compared to the plastic in terms of: Pulse Shape Discrimination (PSD) with a Figure Of Merit (FOM) of 1.5 vs. 1.1, energy resolution (15% vs 20% at 662 keV) and fast neutron efficiency (12% vs. 9% with an AmBe source). For both scintillators, the dose rate response is linear up to 1 mSv/h with a ^{137}Cs γ-ray source. With a neutron source, the response is linear, and the FOM is almost constant for dose rates up to 1.5 mSv/h. The PUR reduces the false neutron events by one order of magnitude when the detectors are irradiated with a γ-ray source up to 10 mSv/h, and it correctly works when irradiated with an AmBe source at 1.5 mSv/h together with a ^{137}Cs source up to 60 µSv/h. The proposed PUR algorithm is promising but needs to be tested with a higher intensity mixed n/γ field. The temperature stability of both detectors was also studied in the temperature range from -10°C to +40°C. The light yield increases by around 25% for both detectors when reducing the temperature. The variation of the neutron count rate is around 10% in the same temperature range. This work provides a complete overview of the performance of these detectors and a coherent comparison between the two types of scintillators with the same experimental setup.

Keywords— Stilbene, EJ-276, SiPM, Fast neutrons, Dose rate.

1. Introduction

Organic scintillators are widely used in particle detection. They are often preferred to inorganic crystals since their fabrication is easier, they have short decay times and lower cost. Moreover, the capability to perform particle discrimination [1] makes them suitable for charged particle detection. As neutron detectors, organic scintillators have been investigated for several applications such as fission neutron detection, fast neutron imaging [2, 3], neutron spectrometry (with unfolding) [4] and as an alternative to ^{3}He counters in non-proliferation application, homeland security and fusion research [5, 6]. In this paper, we consider the stilbene and EJ-276 (plastic) organic scintillators for a neutron probe of the B-RAD [7, 8], a radiation survey meter developed by CERN and the Polytechnic of Milan and commercialized by ELSE NUCLEAR [9].

The B-RAD is specifically designed for operation in strong magnetic fields. Its detection system consists of a scintillator (currently a $LaBr_3$ crystal for γ dose rate and γ-spectrometry) coupled with a Silicon Photomultiplier (SiPM) array, instead of a traditional Photomultiplier Tube (PMT), and specifically designed electronics. The purpose of this paper is to study two potential candidates for an additional probe for fast neutron measurements.

Here, we analyse and compare the main features of the stilbene and EJ-276 coupled with a large area SiPM array. The scintillators and the experimental setup are described in section 2. Section 3 addresses the energy calibration and energy resolution, the neutron/γ–ray (n/γ) discrimination via the Pulse Shape Discrimination (PSD) technique, the count rate linearity, the neutron detection efficiency, a Pile-Up Rejection (PUR) algorithm developed for application in high-intensity and mixed radiation fields and the temperature dependence. The results are discussed and compared with literature data when available. Finally, the conclusions are summarized in section 6.

2. Detectors and experimental setup

The stilbene and the EJ-276 are organic scintillators characterised by a similar chemical composition, low density (close to 1 g cm^{-3}) and short scintillation decay times (less than 500 ns). Table 1 summarizes and compares the main properties of the two scintillators. The quenching factor for recoil protons is also reported in view of their application as fast neutron detectors.

Table 1. Comparison of the main properties of the stilbene and EJ-276 scintillators.

	Stilbene	**EJ-276**
Manufacturer	Inrad Optic	Scionix
Type of scintillator	Organic crystal	Organic plastic
Shape and dimensions	1–inch right cylinder	1–inch right cylinder
Chemical composition	$C_{14}H_{12}$ [10]	4.546×10^{22} H atoms cm^{-3} 4.906×10^{22} C atoms cm^{-3} [11]
Density	1.15 g cm^{-3} [10]	1.096 g cm^{-3} [11]
Housing	Yes	No (wrapped in Teflon tape)
Peak scintillation wavelength	390 nm [10]	425 nm
Scintillation light yield	14,000 ph MeV^{-1} [10]	8,600 ph MeV^{-1} [11]
Decay constants [ns]	4, 35, 332 [12]	13, 35, 270 (γ) 13, 59, 460 (n) [11]
Recoil proton quenching factor [(1)] (proton recoil energy)	0.1 – 0.17 [13] (300 keV – 3 MeV)	0.08 – 0.3 [(2)] [14] (300 keV – 3 MeV)

The scintillators were coupled with an 8×8 SiPM Array J-30035-64P from SensL [15, 16] through optical grease and placed inside a light-tight box. A bias voltage of +28.5 V, corresponding to 4 V of overvoltage, was supplied to the SiPM array. The Photon Detection Efficiency (PDE) for the selected overvoltage is around 40% for the stilbene and 43% for the EJ-276 [16].The summed anode signal was acquired with a suitably designed board [17, 18] and sent to a CAEN DT5720 digitizer (12 bit, 12 Ms/s). The digitizer threshold was set at 100 keVee for the stilbene and 250 keVee for the EJ-276. The measurements described in section 3.3 were carried out sending the output signal to a Teledyne LeCroy Waverunner 8104 Oscilloscope (1 GHz, 20 Gs/s) with a 50 Ω

(1) The quenching factor is defined as E_{vis}/E_r where E_{vis} is the energy in electron equivalent measured with the scintillator after γ-ray calibration and E_r the energy of the recoil proton emitted by the neutron reaction.
(2) Data have been extrapolated from the light yield data relative to 477 keVee.

termination (instead of the digitizer) because it allows a higher sampling frequency and more flexibility of parameter setting. Around 30,000 signals were saved for each measurement and analysed offline with a Python code [19].

3. Characterisation of the stilbene and the EJ-276 scintillators

3.1 Energy calibration and energy resolution

Organic scintillators such as the stilbene and the EJ-276 (see Table 1) are made of low Z materials and have low density. Therefore, their interaction with γ-rays mainly occurs through Compton scattering [1]. Because of the lack of the photoelectric peak, the Compton edge has to be assumed as reference point for the energy calibration. However, one of the major obstacles is to accurately set its position [20–23]. In this work, the energy calibration was performed according to the following method [23]. The spectra of three γ-ray sources (^{137}Cs, ^{60}Co and ^{22}Na) were acquired. The theoretical spectra of ^{137}Cs, ^{60}Co and ^{22}Na in the stilbene and EJ-276 scintillators were calculated using the FLUKA Monte Carlo code version 4-0.1 [24–26]. A Gaussian Energy Broadening (GEB) was applied to the simulated spectra to take into account the finite energy resolution of the detectors assuming a σ proportional to $\sqrt{E}$, where E is the γ-ray energy [22]. In analogy with [22], the energy resolution is defined as R_E = FWHM/E, where FWHM is the Full Width at Half Maximum. The broadened spectrum was normalized to the maximum of the experimental Compton distribution and its x-axis (in energy scale) was linearly scaled in order to match the experimental spectrum (in ADC channels). Both the scaling factor and the R_E values were varied to find the broadened spectrum, which best fitted the experimental one (through least square minimization) in the Compton edge area.

Figure 1 shows the three spectra (experimental, simulated and broadened) of ^{137}Cs and ^{60}Co for the stilbene in the top, and the plots of the residuals between the experimental and broadened spectra in the bottom, in the selected energy range. Figure 2 shows the same results for the EJ-276. The position of the Compton edge of ^{137}Cs (447 keV) for the stilbene and EJ-276 was found at 92% and 90% of the position of the maximum, respectively (at 74% and 73% of the peak height). For the EJ-276, the two Compton edges of ^{60}Co were not well distinguishable in the experimental spectrum. For this reason, a single fit was performed and the position of the mean energy of the two Compton edges was considered as the calibration point (i.e. 1041 keV) [27]. Figure 3 shows the calibration points and the linear fits for both scintillators. Table 2 reports the linear fitting equations and the corresponding R^2. The different slopes of the energy calibration equations for the two scintillators are in agreement with the different light yields (see table 1). The small intercept is also expected since it is due to the non-linearity of the light yield at low energies (below 100 keVee) [28].

The calculation of the energy calibration and the energy resolution in organic scintillators is not unique as explained in [27]. In this study, the energy resolution for the stilbene and the EJ-276 scintillators is 15% and 20% respectively. From the plots of the residuals, the Compton edges are well fitted in the selected energy ranges, and the comparison between the two detectors is reliable. The fitting region was restricted to the Compton edge range since the photon backscattering and the source geometry, which affect the spectrum shape below the Compton edge, were not considered. A few percent variation on the energy resolution is acceptable for the scope of this study since the two detectors were studied for use in a dose rate survey meter.

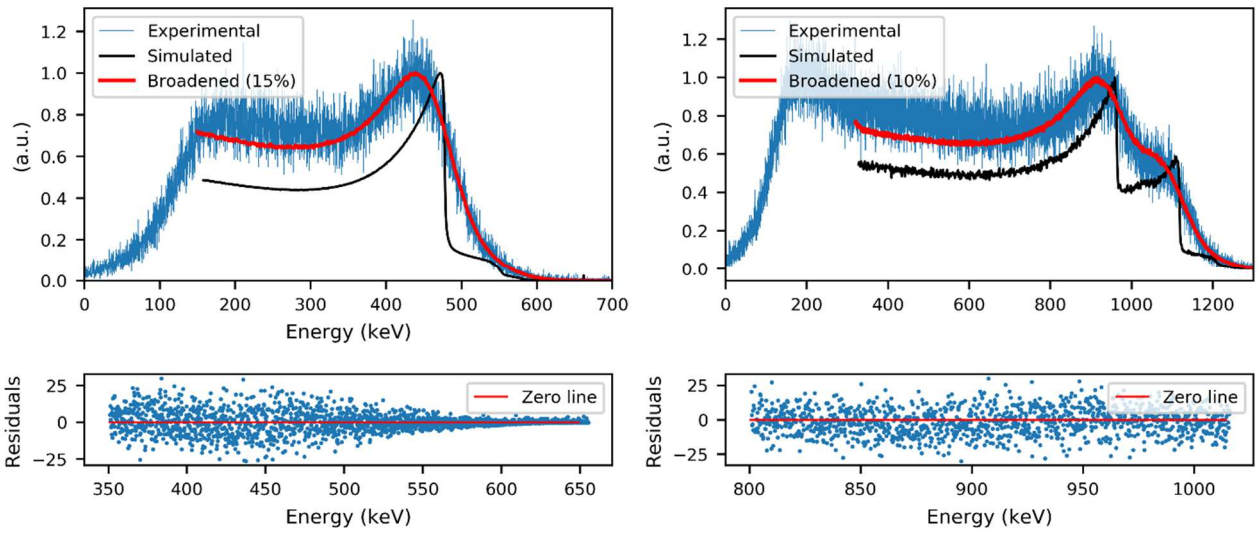

Figure 1. Comparison of the normalized spectrum of a ^{137}Cs source (on the left) and of a ^{60}Co source (on the right) measured with the stilbene scintillator (blue line), the FLUKA simulated spectrum (black line) and the result of the GEB of the simulated spectrum which best fits the experimental data (red line). On the bottom, the plots of the residuals between the experimental and broadened spectra.

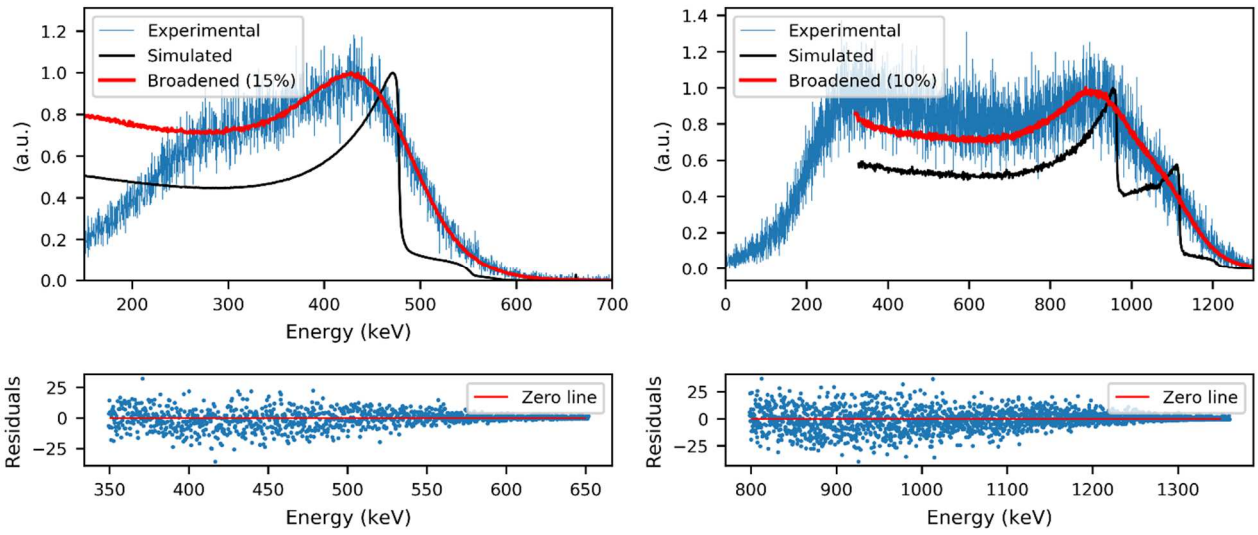

Figure 2. Comparison of the normalized spectrum of a ^{137}Cs source (on the left) and of a ^{60}Co source (on the right) measured with the EJ-276 scintillator (blue line), the FLUKA simulated spectrum (black line) and the result of the GEB of the simulated spectrum which best fits the experimental data (red line). On the bottom, the plots of the residuals between the experimental and broadened spectra.

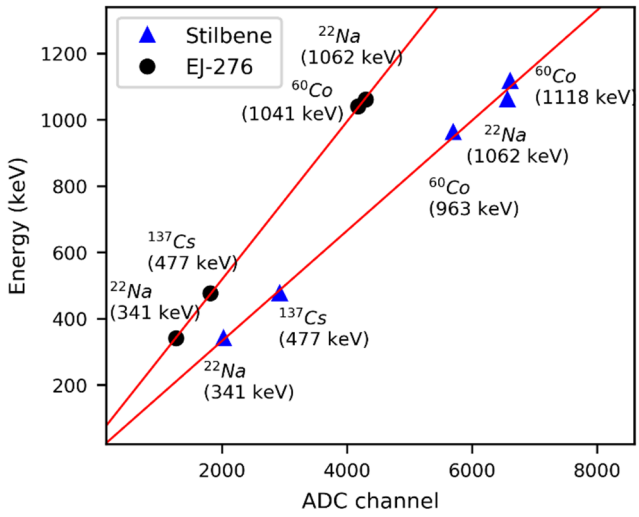

Figure 3. Compton edge positions of ^{137}Cs, ^{60}Co and ^{22}Na sources for the stilbene and EJ-276 scintillators. The red lines show the linear fits to the data points.

Table 2. Energy calibration equation for the stilbene and EJ-276, where E is the energy in keV and ch. the corresponding channel. The R^2 of the linear regression is also reported.

	Equation	R^2
Stilbene	E (keV) = (0.166±0.005) × ch. + (0.952 ±27.426)	0.998
EJ-276	E (keV) = (0.238±0.002) × ch + (42.440 ±5.507)	0.999

3.2 Pulse Shape Discrimination (PSD)

The PSD capability is one of the most interesting parameters for a neutron detector. In this work, the PSD was defined according to the charge integration method and calculated for each signal as follows:

$$PSD = \frac{Q_{long} - Q_{short}}{Q_{long}} \qquad (1)$$

where Q_{short} and Q_{long} are the integrals of the signal (i.e. the charge) calculated over two different integration times (t_{short} and t_{long} respectively). A Figure of Merit (FOM) is defined to quantify the goodness of the PSD according to Eq. 2:

$$FOM = \frac{x_n - x_\gamma}{FWHM_n + FWHM_\gamma} \qquad (2)$$

where x_n and x_γ are the mean values of the gaussian fitting equations of the neutron and γ-ray distributions respectively, and $FWHM_n$ and $FWHM_\gamma$ the corresponding FWHM.

In the present work, the PSD analysis was performed with the DPP-PSD software provided with the CAEN digitizer. The FOM was 1.5 for the stilbene and 1.1 for the EJ-276 scintillator. In the latter case, a higher energy threshold of 350 keVee had to be set to reach a sufficient discrimination

(FOM > 1.15), while it was not necessary for the stilbene. The time windows were selected so as to optimize the FOM and set at 300 ns and 3 µs for both scintillators. The long-time gates selected in this work, if compared to the decay times of both scintillators (see table 1), are due to the high capacitance of the 64 pixels array, which dominates the shape of the output pulse.

Table 3 compares the FOM calculated in this work with the one derived in other studies. The FOM found in this work is within the range of values found in the literature. The deviation from the best FOM can be explained by the different energy threshold and/or by the use of a different photodetector.

Table 3. Comparison between the FOM calculated in this work and literature data. The size of the scintillator, the photodetector and the source are specified. The energy cut-off or the energy range selected for the PSD calculation are given in brackets.

	This work	Steinberger et al. [29]	Taggart et al. [30]	Grodzika-Kobylka et al. [31]
Dimensions	Ø1 inch × 1 inch cylinder	6 mm × 6 mm × 50 mm	6 mm × 6 mm × 6 mm	Ø1 inch × 1 inch cylinder
Photodetector	64 pixels J-Series SiPM array	SensL C-Series SiPM	J-series SiPM (single pixel)	R6233-100 Hamamatsu PMT
Source	AmBe	^{252}Cf	AmBe	PuBe
FOM Stilbene	1.5 (100 keVee)	1.17 (100 – 200 keVee)	–	1.74 (100 keVee)
FOM EJ-276	1.1 (250 keVee)		2.39 (500 – 600 keVee)	1.09 (100 keVee)

3.3 Count rate linearity

The count rate as a function of the dose rate of both detectors was measured. As expected, the count rate linearly increases with the dose rate up to a limit where the count rate starts to saturate because of pile-up events. The pile-up also affects the PSD analysis when the detectors are exposed to a mixed n/γ radiation field. This effect was also studied. It is worth mentioning that the results presented in this work are mainly affected by the electronic read-out system (i.e. the 64 pixels array) and by the selected PSD parameters. However, they can be used for comparison with similar detectors, especially because of the lack in the literature of data measured with similar photodetectors (large SiPM array).

The scintillators were exposed to different photon dose rates from a ^{137}Cs source at the Calibration Laboratory of the Radiation Protection group at CERN [32], from 1 µSv/h to 15 mSv/h. For both detectors, count rate saturation effects start at around 1 mSv/h, which corresponds to 4×10^4 and 3×10^4 counts per seconds (cps) in the stilbene and EJ-276, respectively. Figure 4 shows the count rate as a function of the dose rate and the linear fitting equations calculated outside the count rate saturation region (for a better visualization the plot in figure 4 starts from 300 µSv/h).

The measurements were repeated with an AmBe neutron source at dose rates between 5 µSv/h and 1.5 mSv/h, which is the maximum available dose rate at the Calibration Laboratory. The neutron count rate was derived from the PSD analysis. Figure 5 shows the results: the left y-axis is the measured count rate, while the right y-axis represents the count rate corresponding to neutron events only calculated after the PSD. As can be seen, the response is linear over the entire range. The maximum count rate is 1.5×10^3 cps and 1.2×10^3 cps for the stilbene and the plastic respectively, quite lower than the count rate saturation value found with the photon source.

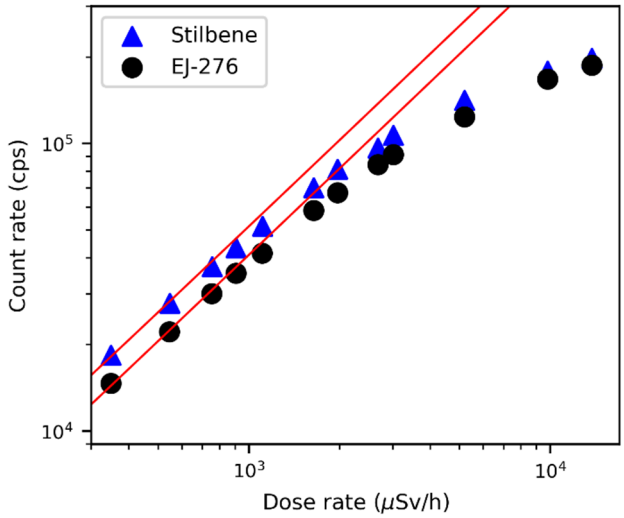

Figure 4. Count rate versus dose rate measured with the stilbene (blue triangles) and the EJ-267 (black dots) scintillators when exposed to photons from a ^{137}Cs source before the count rate saturation region. The red line represents the linear fits calculated outside the count rate saturation region to the data points. The error bars are smaller than the data points.

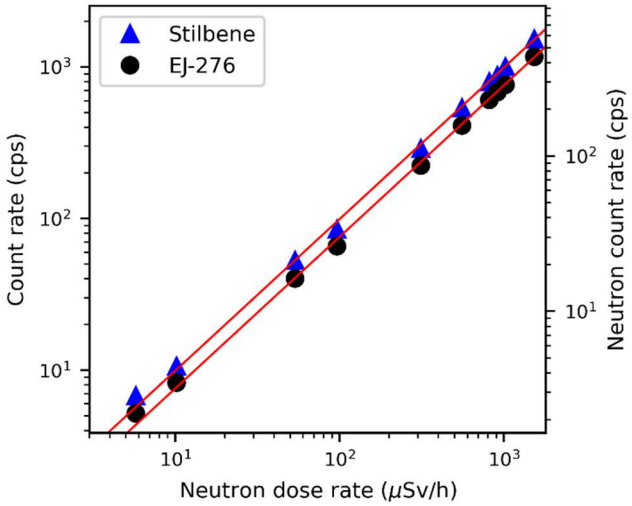

Figure 5. On the left y-axis, count rate versus dose rate measured with the stilbene (blue triangles) and the EJ-267 (black dots) scintillator when exposed to an AmBe neutron source. On the right y-axis the neutron count rate calculated after the PSD analysis for the same measurements. The red lines represent the linear fits to the data points. The error bars are smaller than the data points.

The variation of the PSD with increasing pile-up was studied by means of the 2D PSD histogram plot. Each detector was first irradiated with the AmBe source alone at the maximum available dose rate, i.e around 1.5 mSv/h. Afterward, the detectors were exposed simultaneously to the ^{137}Cs and AmBe sources. The neutron source activity and the source to detector distance were kept constant to maintain the neutron dose rate at 1.5 mSv/h, whereas the photon dose rate was progressively increased by increasing the source activity. Figures 6, 7 and 8 compare the 2D histogram of the PSD vs. energy measured with the stilbene at around 1×10^3 cps, 5×10^3 cps and 40×10^3 cps, respectively. At 5×10^3 cps (figure 7) many pile-up events are detected in the energy range of the

^{137}Cs source, which become dominant at 40×10^3 cps. The same behaviour is observed with the EJ-276 starting from 3.5×10^3 cps. Figures 7 and 8 clearly show that the signals affected by pile-up are spread along the entire PSD range leading to a bad discrimination and to a completely wrong estimation of the dose rate if the energy threshold is not modified.

The PSD was also monitored by calculating the FOM while keeping constant the energy threshold of each detector. Above 3×10^3 cps the FOM drastically drops compared to the value calculated below 1.5×10^3 cps, where the variation between the maximum and the minimum value is about 5%. A correct discrimination can be restored, for example by increasing the energy threshold, as can be seen in figure 7, where the discrimination is still feasible if the energy threshold is set above 1.5 MeV.

As stated before, the count rate range in our detectors is mainly limited by the high capacitance of the employed photodetector. For this reason, it can be extended simply by using a PMT in place of the large area SiPM array. This option was not considered since the B-RAD is designed to work in high magnetic field regions and a PMT cannot be employed. A PUR algorithm was instead tested as discussed in the following section.

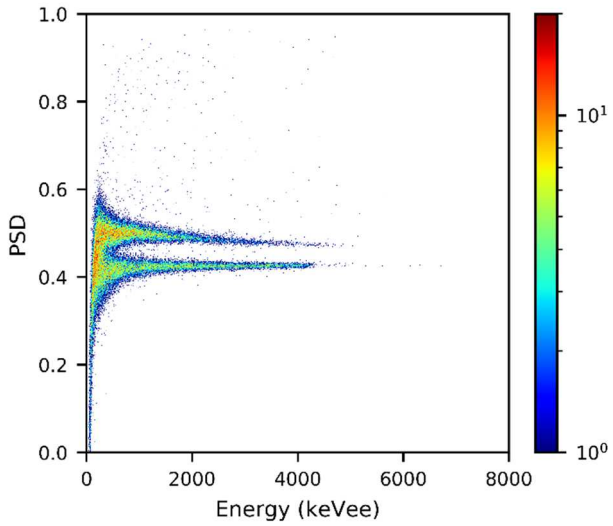

Figure 6. 2D histogram plot of the PSD for the stilbene when irradiated with an AmBe neutron source at 1.5 mSv/h (around 1,000 cps).

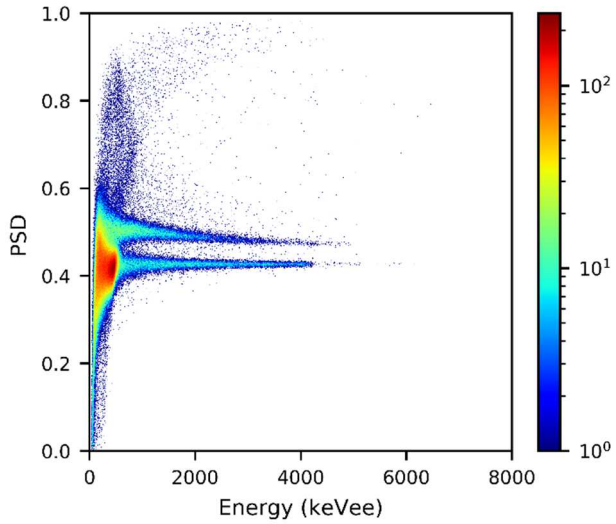

Figure 7. 2D histogram plot of the PSD for the stilbene when irradiated with an AmBe neutron source at 1.5 mSv/h and a ^{137}Cs photon source at 60 µSv/h (around 5,000 cps).

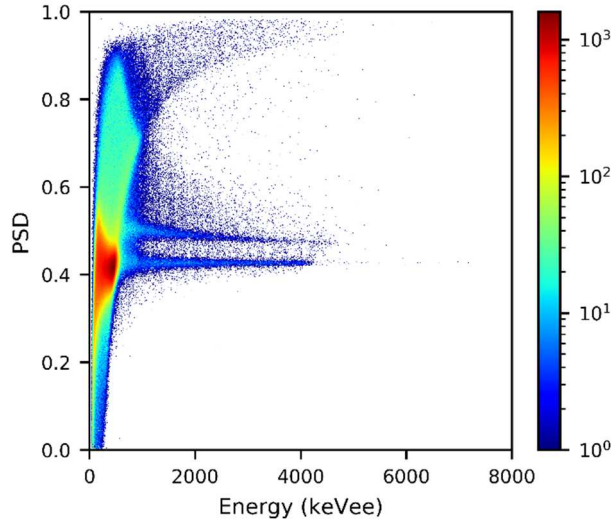

Figure 8. 2D histogram plot of the PSD for the stilbene when irradiated with an AmBe neutron source at 1.5 mSv/h and a ^{137}Cs photon source at 650 µSv/h (around 40,000 cps).

3.4 Pile-up rejection (PUR)

A PUR algorithm was developed to improve the PSD analysis and increase the count rate linearity of the two detectors. The PUR algorithm was defined similarly to the fractional double-pulse technique described in [5, 6]: a pulse is classified as double if consecutive samples (points of the digitalized pulse) exceed a certain fraction of the pulse height in the tail region. The algorithm was tested for a single combination of the parameters (time windows and threshold) since the results were sufficiently good and proved the possibility to apply the proposed PUR. However, for its application in the B-RAD, these parameters must be optimised.

The time windows were selected by a qualitative analysis, i.e. by observing the neutron and photon standard pulses (see figure 9). For both scintillators, the tail region was selected starting from 1 µs (indicated by the dashed black vertical line in figure 9) and the total recorded length was set at 4 µs.

The threshold (represented by the horizontal line in figure 9) was selected as the fraction of the γ-ray pulse amplitude at 1 μs with respect to the pulse height. The number of samples was chosen to exceed the time interval between the dashed black and dashed-dotted red vertical lines in figure 9. The latter was selected as the point where the neutron pulse crosses the threshold. Following this approach, the threshold was set at 19% and 21% of the pulse height, for the stilbene and the EJ-276, respectively. The sampling frequency was set to 250 MHz for both scintillators.

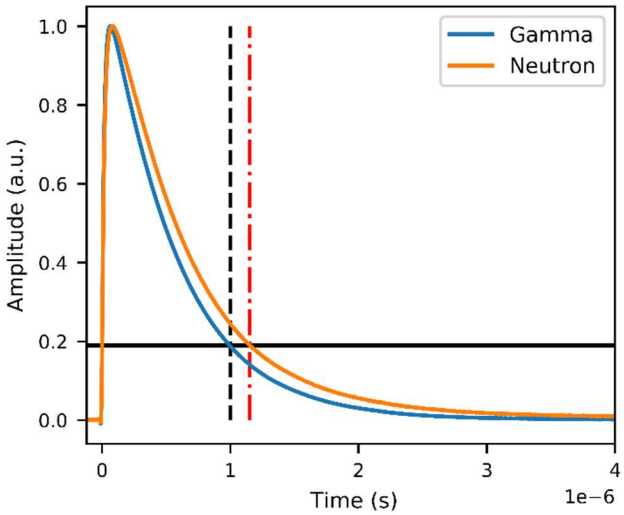

Figure 9. The neutron and γ-ray standard pulses in stilbene. The horizontal line represents the amplitude threshold selected for the PUR, the vertical lines the minimum time intervals that the signal amplitude must exceed, in the tail region, to be discarded by the PUR.

At first, the PUR was applied after irradiating the detectors with a ^{137}Cs source in the 1 μSv/h - 15 mSv/h range. Figures 10 and 11 show the 2D histogram plots acquired with the stilbene before and after applying the PUR at 1 mSv/h. One should note that γ-ray events are expected in the bottom region of the plot, delimited in figures 10 and 11 by the continuous red line. Figure 10 shows that because of pile-up γ-ray events are erroneously classified as neutron events, while figure 11 demonstrates that the PUR correctly removes them. In analogy to [5] the erroneous classification ratio (ER) was calculated as the ratio between the signals detected in the neutron region over the total detected pulses, before and after the PUR. The results are plotted in figures 12 and 13 for the stilbene and the EJ-276, respectively. At low dose rate, the stilbene is characterised by an ER one order of magnitude lower than the EJ-276, while for both detectors the ER decreases by a factor of 10 after the PUR, also at high dose rates. The two curves of the ER after the PUR seem to saturate above 1 mSv/h. This is probably due to the spreading of the pile-up events along the entire PSD range, i.e., also in the γ-ray region (below the continuous red line in figures 10 and 11)

A corrected ER factor (ER_{cor}) was defined as the ratio between the signals detected in the neutron region over the signals detected in the region delimited by the γ-ray distribution, confined in figures 10 and 11 by the continuous and dashed red lines. The ER_{cor} is also plotted in figures 12 and 13 (red crosses). The ER_{cor} is linear up to 10 mSv/h for both detectors. Above this value it starts to saturate for the EJ-276 probably because pile-up events are also detected inside the γ-ray region, which cannot be discriminated by the PUR. However, the PUR is still able to well discard false events in the neutron region.

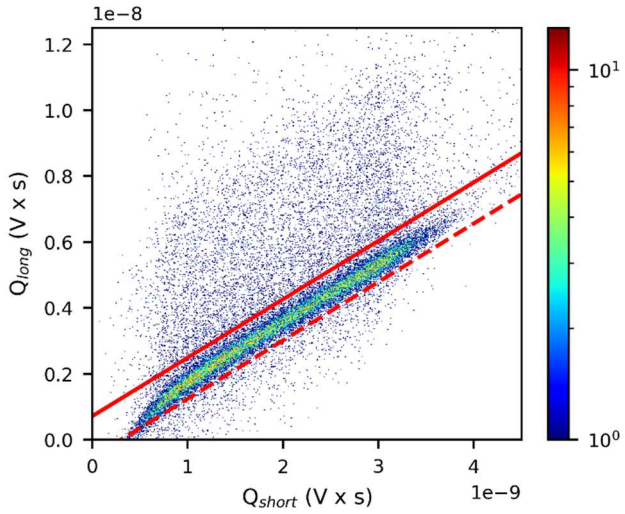

263

264 *Figure 10. The Q_{long} vs Q_{short} 2D histogram plot of the stilbene irradiated with a ^{137}Cs source at*
265 *1 mSv/h. The two red lines delimit the γ-ray region.*

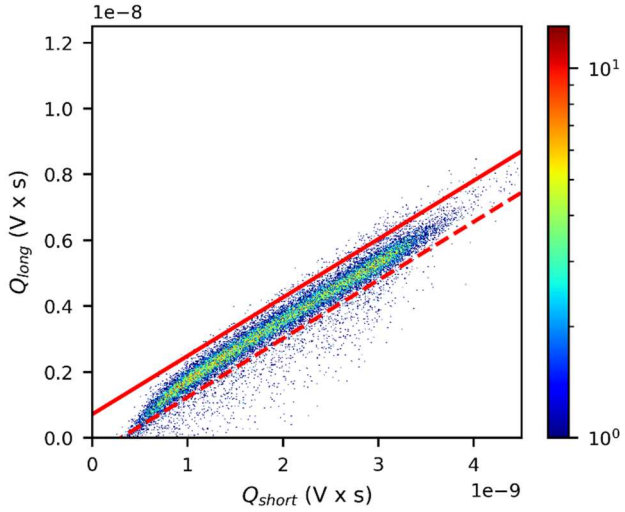

266

267 *Figure 11. The Q_{long} vs Q_{short} 2D histogram plot of the stilbene irradiated with a ^{137}Cs source at*
268 *1 mSv/h after applying the PUR algorithm. The two red lines delimit the γ-ray region.*

269

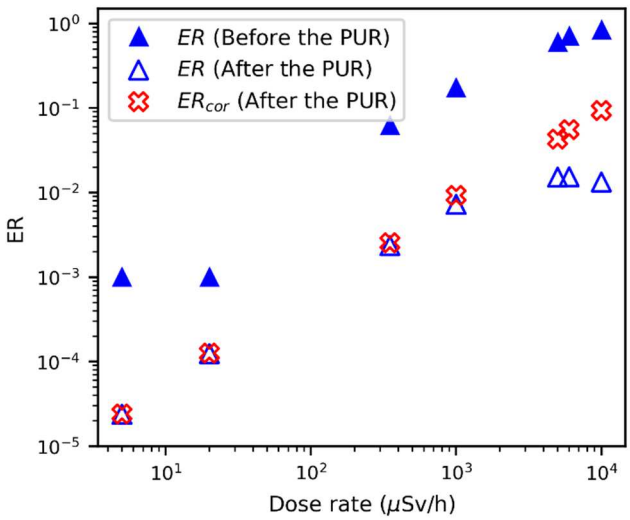

Figure 12. The ER and the ER_{cor} for the stilbene irradiated with a ^{137}Cs at different dose rate values, before and after applying the PUR algorithm.

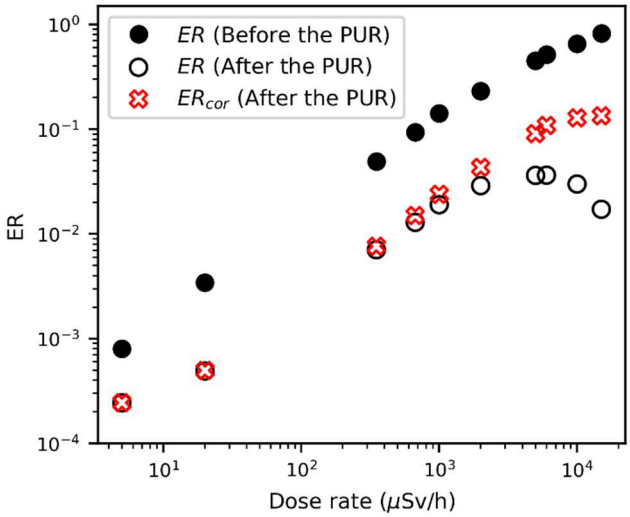

Figure 13. The ER and the ER_{cor} for the EJ-276 irradiated with a ^{137}Cs at different dose rate values, before and after applying the PUR algorithm.

The PUR was also tested in a mixed n-γ field from an AmBe source, at around 1.5 mSv/h, and from a ^{137}Cs source, at 5 μSv/h and 60 μSv/h. Figures 14 and 15 show the PSD plot before and after the PUR for the stilbene for the two cases. The green lines were calculated from the PSD plot (Q_{long} vs Q_{short}) acquired with the AmBe source alone as the lines which enclose the region of the neutron signals. As can be seen, the PSD is dominated by the ^{137}Cs signals, especially with the 60 μSv/h ^{137}Cs source, however the AmBe source is still detected below the ^{137}Cs distribution. The tails of the neutron and γ-ray distributions can be identified. After applying the PUR, the pile up signals are correctly rejected. In fact, more than 95% of the signals above the neutron region are always discarded. With the 5 μSv/h ^{137}Cs source, less than 5% of the signals inside the neutron region are erroneously rejected, whereas with 60 μSv/h source the rejection rate is around 20% for the stilbene and 50% for the EJ-276. Nonetheless, neutrons from the AmBe source are still detectable in spite of the low n/γ ratio.

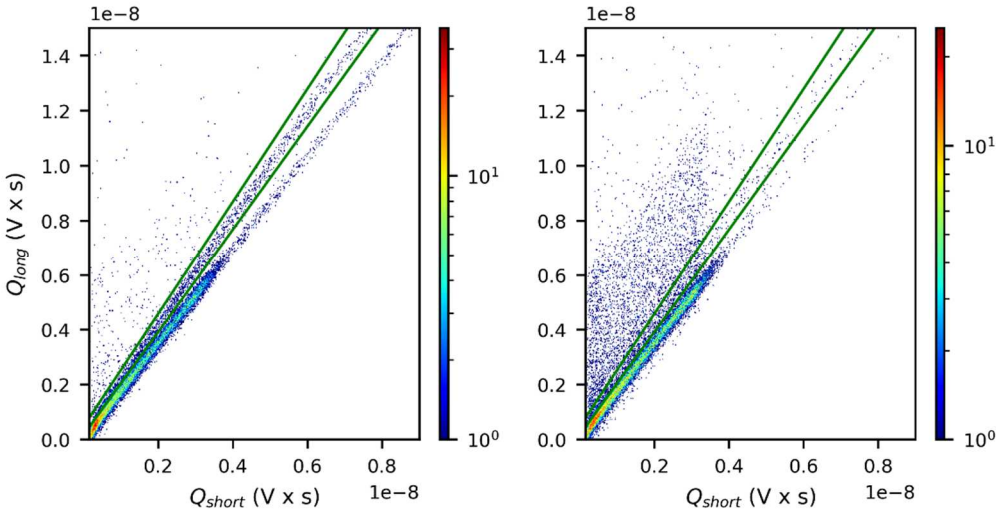

Figure 14. The Q_{long} vs Q_{short} 2D histogram plot for the stilbene irradiated with an AmBe source (at 1.5 mSv/h) and a ^{137}Cs source (at 5 µSv/h on the left and at 60 µSv/h on the right), before applying the PUR algorithm. The green lines delimit the detected neutron signals.

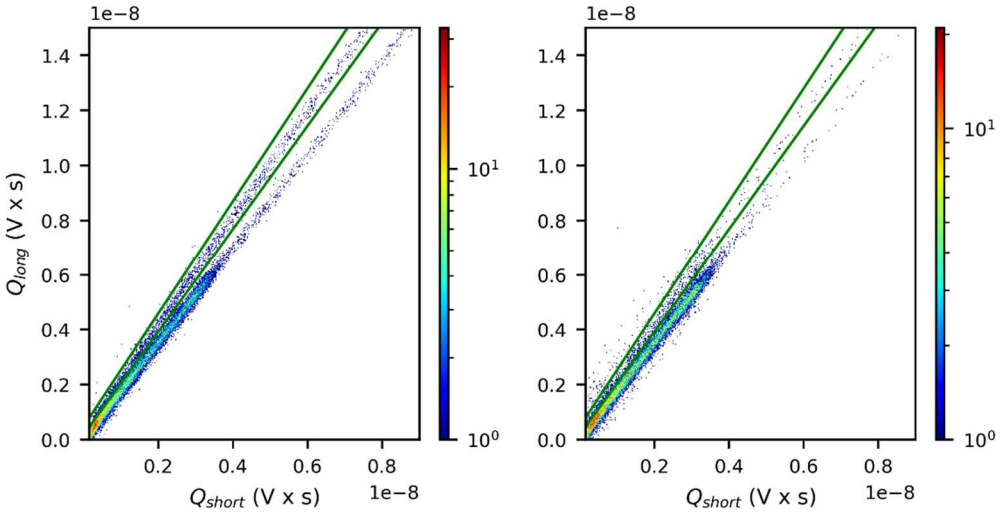

Figure 15. The Q_{long} vs Q_{short} 2D histogram plot for the stilbene irradiated with an AmBe source (at 1.5 mSv/h) and a ^{137}Cs source (at 5 µSv/h on the left and at 60 µSv/h on the right), after applying the PUR algorithm. The green lines delimit the detected neutron signals.

Due to the lack of data measured with similar photodetectors (large SiPM arrays), the study of the linearity and the pile-up events was performed using as a reference the work by Bourne et al. [5]. Bourne et al. coupled a Ø5.08 cm × 5.08 cm cylindrical stilbene scintillator with a PMT. They demonstrated that their detection system is still able to detect neutrons when exposed to a radiation field of 1000 γ-rays per neutron impinging on the detector (with a maximum count rate of 10^5 cps), by implementing a more sophisticate PUR technique. The lower limit set in this work (at around 3-4 × 10^3 cps) with respect to Bourne et al. is mainly due to the longer time profile of the signal produced by the SiPM array as compared to the PMT (the time window in [5] was 300 ns while in this work it was set to 4 µs). Below this limit, the proposed PUR algorithm is promising for application in neutron dose rate meters. Due to the dead time of our acquisition system, mainly

induced by the oscilloscope, at higher count rates the number of detected neutrons (among 30,000 signals) was too low to evaluate the efficiency of the PUR.

3.5 Neutron detection efficiency

The neutron detection efficiency was calculated as the average of the intrinsic neutron efficiencies (ε) (as defined in [33]) measured in the linear range between 5 µSv/h and 1.5 mSv/h (see figure 4). The obtained values are 12% for the stilbene and 9% for the plastic, which correspond to 2.0 counts per nSv and 1.1 counts per nSv, respectively.

It should be noted that the calculated efficiencies are hugely affected by the threshold because the pulse height spectrum in organic scintillators has a continuum shape and hence, all the counts below the threshold are not counted. If we apply the same energy threshold to both scintillators, e.g. 250 keVee, which is the minimum threshold for the EJ-276, the calculated efficiency of the two detectors is comparable: 1.1 counts per nSv for the EJ-276 and 1.3 counts per nSv for the stilbene.

3.7 Temperature dependence

Both detectors, inside the light-tight box, were placed in a climate chamber in which the temperature was varied from -10°C to +40°C at a rate of 10°C h^{-1}. Measurements were performed in 10°C steps with a ^{137}Cs and an AmBe source independently. A thermocouple was placed close to the SiPM because of the different thermal inertia of the detector inside the box and the climate chamber.

The temperature dependence of the detectors depends on both the variation of the scintillators' light yield and the breakdown voltage. The combined effect was evaluated by measuring the variation of the Compton edge position (in the ^{137}Cs spectrum), calculated as described in section 3.1.

The contribution of the SiPM was calculated as in [34], considering that the breakdown voltage increases with temperature at a rate of 21.5 mV $°C^{-1}$ and the gain linearly decreases accordingly [16]. The contribution of the SiPM to the variation of the Compton edge position was assumed proportional to the gain variation. Finally, the contribution of each scintillator was obtained from the comparison of the measured and calculated variation of the Compton edge position. Please note that the former is ascribed to the SiPM + scintillator system, while the latter is attributed to the SiPM only.

Figure 16 compares the variation of the measured and calculated Compton edge position for both detectors. The x-axis is the temperature measured by the probe close to the SiPM. For the stilbene, below ~20°C the measured Compton edge position linearly decreases with temperature with a slope of -18.7 $\pm$ 0.4 channel $°C^{-1}$ versus a variation of -12.7 channel $°C^{-1}$ due to the SiPM only, i.e. the light yield of the stilbene decreases inducing a faster variation of the Compton edge position. Above 20°C the stilbene light output increases and partially compensates the SiPM effect.

Similarly, for the EJ-276, the Compton edge position decreases below 20°C (see figure 16). Nonetheless, the difference between the measured and calculated curves is smaller: -10.5 $\pm$ 0.6 channel$°C^{-1}$ versus -7.6 channel $°C^{-1}$ respectively. Above 20°C, the temperature dependence is mainly attributed to the SiPM. This is partially in agreement with [35], where the variation of the Compton edge position measured by a PMT with a plastic scintillator is almost flat in the temperature range - 30°C – 20°C. However, in [35] the exact composition of the plastic scintillator is not specified. The total percent variation of the Compton edge position is around 25% for both detectors.

The variation of the PSD capability was also investigated with the AmBe source by observing both the variation of the PSD distribution, and of the FOM. Figure 17 shows the PSD distribution at different temperatures for the stilbene and the EJ-276, and figure 18 compares the variation of their FOM. In figure 17, the left and right Gaussian distributions (on both plots) are associated to γ-rays and neutrons respectively.

In both detectors, up to 20°C, the shape of the PSD distribution remains unchanged but, as expected, the number of counts decreases with temperature because of the increasing breakdown voltage. For the stilbene, at 30°C and 40°C, the neutron distribution shifts to the right and the right tail of the γ-ray distribution increases. The intensity of the fast decay appears to decrease with temperature in favour of the slow component (according to equation 1). This effect is generally possible since the temperature can affect different scintillation mechanisms in different ways. For the EJ-276, the PSD distribution above 20°C shows an opposite trend as compared to the stilbene. The peaks of the two Gaussians slightly move to the left and in addition, some signals are detected in the region between the two distributions. At higher temperatures, the lower light yield of the EJ-276 combined with the higher breakdown voltage of the SiPM has a large impact on the PSD analysis. A greater number of signals is in fact detected just above the digitizer threshold and it is well known that for low amplitude signals the discrimination is not clear. To overcome this limit and for a better comprehension, a higher bias voltage can be set in the EJ-276 detector. For both scintillators the temperature increase induces a broadening of the neutron and γ-ray distributions in the PSD plot resulting in the decrease of the FOM (see figure 18).

To our knowledge, the variation with temperature of the light yield in organic scintillators has not been quantified yet. Baker et al. [36] reported a weak decreasing trend of the stilbene light yield with increasing temperature between -90 – 70°C, partially in agreement with this work. In [36] the stilbene was irradiated both with a γ-ray source and a neutron source. A study was performed with an anthracene crystal (comparable to the stilbene) in [37] only for a 6°C temperature range (22 – 28°C) and only for γ-ray detection. In this study, a slightly linear decreases of the light output was measured of less than 10%. In [35], the temperature dependence of the stilbene is deeply investigated between -30°C and 60°C and the pulse shapes at different temperature are also reported. The pulse shape seems to be constant in the abovementioned range. However, the discussion is lacking and a more accurate study is necessary (e.g. fitting of the average signals). On the other hand, the light yield of plastic scintillators was considered temperature independent [38] until recent studies have demonstrated some dependence [39,40]. In [40], a small or almost null temperature dependence was measured for some plastic scintillators according to the substrate material.

Figure 19 shows the variation of the neutron counts with temperature (15 minutes of acquisition time). The variation of the neutron counts with temperature is around 10% for both detectors, which is still acceptable for applications in radiation protection. The measured neutron counts with the stilbene has a minimum at 10°C, while the EJ-276 is almost flat up to 20°C and shows a decreasing trend above that temperature. This variability makes the temperature correction not an easy task. Further investigation such as measurements with a PMT and a pulse shape analysis should be performed.

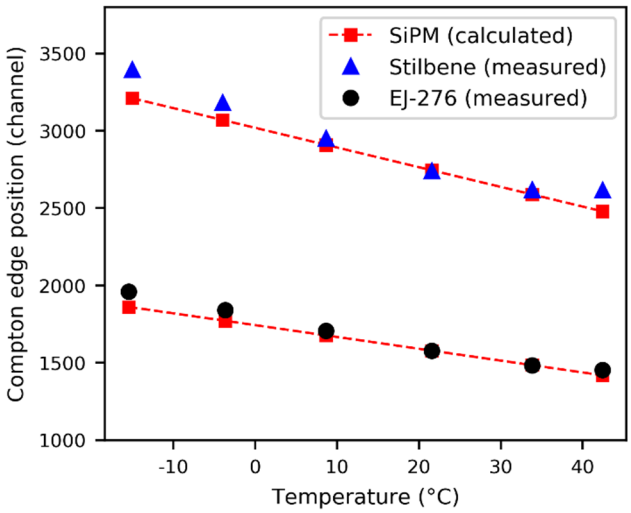

Figure 16. Variation with temperature of the Compton edge position of a ^{137}Cs source for the stilbene and the EJ-276. The x-axis is the temperature measured by a thermocouple close to the SiPM array while the temperature chamber was varied between -10°C and +40°C. The error bars are smaller than the data points.

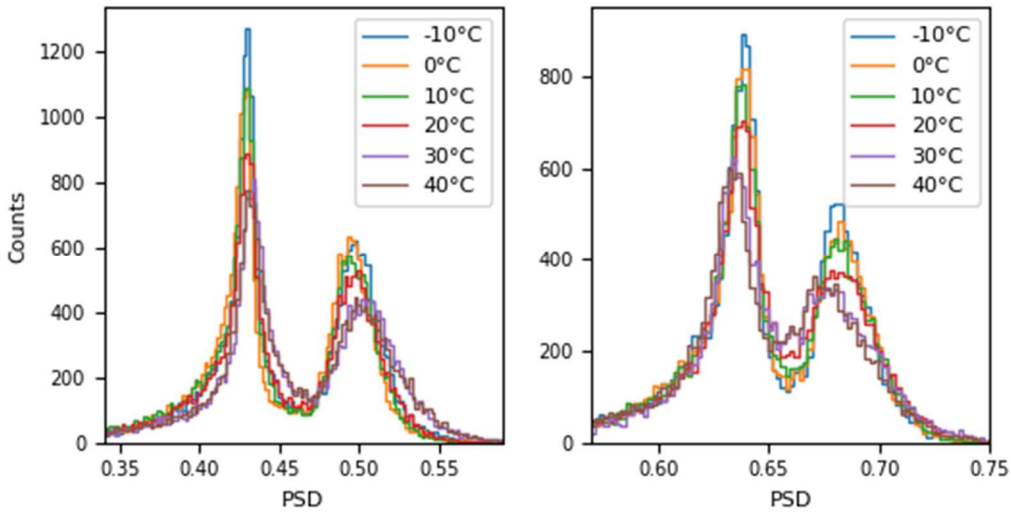

Figure 17. Variation of the PSD distribution measured with an AmBe source with the stilbene (left) and the EJ-276 (right) while the temperature varied between -10°C and +40°C.

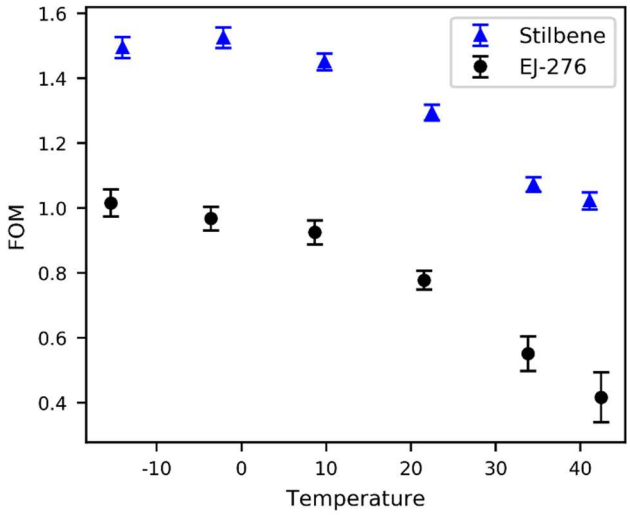

Figure 18. Variation with temperature of the FOM measured with an AmBe source for the stilbene and the EJ-276. The x-axis is the temperature measured by a thermocouple close to the SiPM array, while the temperature in the chamber varied between -10°C and +40°C.

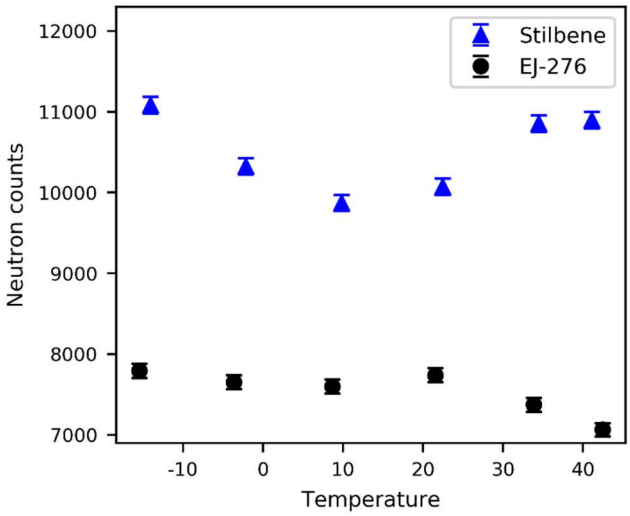

Figure 19. Variation with temperature of the measured neutron counts (15 minutes of acquisition time) with an AmBe source for the stilbene and the EJ-276. The x-axis is the temperature measured by a thermocouple close to the SiPM array while the temperature in the chamber varied between -10°C and +40°C.

6. Conclusions

In this paper, we evaluate and compare the performance of a stilbene and an EJ-276 plastic scintillators coupled with an 8 × 8 SiPM array J-30035-64P from SensL, in view of their potential application in the B-RAD portable survey meter for fast neutron detection. The reported results show that the energy resolution is 15% for the stilbene and 20% for the plastic with a ^{137}Cs source. Moreover, the stilbene shows a better PSD capability compared to the EJ-276: a FOM of 1.5 is achieved with the minimum threshold of 100 keVee, while a threshold of 350 keVee had to be set to reach a sufficient discrimination with the plastic (FOM = 1.15). The calculated neutron detection efficiency is 12% for the stilbene and 9% for the plastic. The response of both detectors starts to deviate from linearity at 1 mSv/h photon dose rate, whereas the PSD is stable up to 1.5 mSv/h

neutron dose rate. When exposed to a mixed n-γ radiation field, the FOM of both scintillators drastically drops above 3 - 4 × 10^3 cps. Below this limit, a Pile-Up Rejection algorithm can reduce the detection of false neutron events by one order of magnitude without affecting the detection efficiency. The two scintillators show similar performance in terms of temperature variation in the range -10°C to +40°C. The variation of the measured Compton edge position is around 25%, while the variation of the neutron count rate is around 10%. A deeper investigation of the PSD distribution as a function of the temperature shows a different behaviour of the two scintillators above 20°C. which has to be confirmed by further measurements.

References

[1] G.F.Knoll, Radiation Detection and Measurements, 4th ed., 2010.

[2] U. Bravar, P.J. Bruillard, E.O. Flückiger, J.R. Macri, M.L. McConnell, M.R. Moser, J.M. Ryan, R.S. Woolf, Design and testing of a position-sensitive plastic scintillator detector for fast neutron imaging, IEEE Trans. Nucl. Sci. 53 (2006) 3894–3903. https://doi.org/10.1109/TNS.2006.886046.

[3] E. Brubaker, J. Steele, Neutron imaging using the anisotropic response of crystalline organic scintillators, IEEE Nucl. Sci. Symp. Conf. Rec. (2010) 1647–1652. https://doi.org/10.1109/NSSMIC.2010.5874055.

[4] Y.A. Kaschuck, B. Esposito, L.A. Trykov, V.P. Semenov, Fast neutron spectrometry with organic scintillators applied to magnetic fusion experiments, Nucl. Instruments Methods Phys. Res. Sect. A Accel. Spectrometers, Detect. Assoc. Equip. 476 (2002) 511–515. https://doi.org/10.1016/S0168-9002(01)01499-1.

[5] M.M. Bourne, S.D. Clarke, N. Adamowicz, S.A. Pozzi, N. Zaitseva, L. Carman, Neutron detection in a high-gamma field using solution-grown stilbene, Nucl. Instruments Methods Phys. Res. Sect. A Accel. Spectrometers, Detect. Assoc. Equip. 806 (2016) 348–355. https://doi.org/10.1016/j.nima.2015.10.025.

[6] M.M. Bourne, S.D. Clarke, M. Paff, A. DiFulvio, M. Norsworthy, S.A. Pozzi, Digital pile-up rejection for plutonium experiments with solution-grown stilbene, Nucl. Instruments Methods Phys. Res. Sect. A Accel. Spectrometers, Detect. Assoc. Equip. 842 (2017) 1–6. https://doi.org/10.1016/j.nima.2016.10.023.

[7] A. Fazzi, M. Silari, Portable radiation detection device for operation in intense magnetic field. CERN/Polytechnic of Milan, joint patent. Patent Grant number 9977134 (13 July 2017).

[8] D. Celeste, A. Curioni, A. Fazzi, M. Silari, V. Varoli, B-RAD: A radiation survey meter for operation in intense magnetic fields, J. Instrum. 14 (2019). https://doi.org/10.1088/1748-0221/14/05/T05007.

[9] Online: Products for nuclear safety, radiation detection and measurement - ELSE Nuclear, http://www.elsenuclear.com/it/ (accessed May 8, 2021).

[10] Online: Scintinel™ Stilbene. https://www.inradoptics.com/scintinel-stilbene (accessed May 8, 2021).

[11] Online: https://eljentechnology.com/products/plastic-scintillators/ej-276 (accessed May 7, 2021).

[12] N. Zaitseva, A. Glenn, L. Carman, H. Paul Martinez, R. Hatarik, H. Klapper, S. Payne, Scintillation properties of solution-grown trans-stilbene single crystals, Nucl. Instruments Methods Phys. Res. Sect. A Accel. Spectrometers, Detect. Assoc. Equip. 789 (2015) 8–15. https://doi.org/10.1016/j.nima.2015.03.090.

[13] Y. Shimizu, M. Minowa, H. Sekiya, Y. Inoue, Directional scintillation detector for the detection of the wind of WIMPs, Nucl. Instruments Methods Phys. Res. Sect. A Accel. Spectrometers, Detect. Assoc. Equip. 496 (2003) 347–352. https://doi.org/10.1016/S0168-9002(02)01661-3.

[14] T.A. Laplace, B.L. Goldblum, J.E. Bevins, D.L. Bleuel, E. Bourret, J.A. Brown, E.J. Callaghan, J.S. Carlson, P.L. Feng, G. Gabella, K.P. Harrig, J.J. Manfredi, C. Moore, F. Moretti, M. Shinner, A. Sweet, Z.W. Sweger, Comparative scintillation performance of EJ-309, EJ-276, and a novel organic glass, J. Instrum. 15 (2020). https://doi.org/10.1088/1748-0221/15/11/P11020.

[15] Online: Products - ON Semiconductor. https://www.onsemi.com/products/sensors/silicon-photomultipliers-sipm/j-series-sipm-array (accessed May 8, 2021).

[16] Online: DS-MicroJseries.pdf (sensl.com) (accessed May 7, 2021).

[17] D. Nesrine, Development of neutron detectors for use in radiation protection, University of Paris-Saclay, 2019.

[18] N. Dinar, D. Celeste, M. Silari, V. Varoli, A. Fazzi, Pulse shape discrimination of CLYC scintillator coupled with a large SiPM array, Nucl. Instruments Methods Phys. Res. Sect. A Accel. Spectrometers, Detect. Assoc. Equip. 935 (2019) 35–39. https://doi.org/10.1016/j.nima.2019.04.099.

[19] G. Van Rossum, F.L. Drake, Python 3 Reference Manual, CreateSpace, Scotts Valley, CA, 2009.

[20] H.H. Knox, T.G. Miller, A technique for determining bias settings for organic scintillators, Nucl. Instruments Methods. 101 (1972) 519–525. https://doi.org/10.1016/0029-554X(72)90040-7.

[21] C.H. Lee, J. Son, T.H. Kim, Y.K. Kim, Characteristics of plastic scintillators fabricated by a polymerization reaction, Nucl. Eng. Technol. 49 (2017) 592–597. https://doi.org/10.1016/j.net.2016.10.001.

[22] S. Ashrafi, M. Ghahremani Gol, Energy calibration of thin plastic scintillators using Compton scattered γrays, Nucl. Instruments Methods Phys. Res. Sect. A Accel. Spectrometers, Detect. Assoc. Equip. 642 (2011) 70–74. https://doi.org/10.1016/j.nima.2011.04.003.

[23] G. Dietze, H. Klein, Gamma-calibration of NE 213 scintillation counters, Nucl. Instruments Methods. 193 (1982) 549–556. https://doi.org/10.1016/0029-554X(82)90249-X.

[24] Online: https://fluka.cern.

[25] T.T. Böhlen, F. Cerutti, M.P.W. Chin, A. Fassò, A. Ferrari, P.G. Ortega, A. Mairani, P.R. Sala, G. Smirnov, V. Vlachoudis, The FLUKA Code: Developments and challenges for high energy and medical applications, Nucl. Data Sheets. 120 (2014) 211–214. https://doi.org/10.1016/j.nds.2014.07.049.

[26] G. Battistoni, T. Boehlen, F. Cerutti, P.W. Chin, L.S. Esposito, A. Fassò, A. Ferrari, A. Lechner, A. Empl, A. Mairani, A. Mereghetti, P.G. Ortega, J. Ranft, S. Roesler, P.R. Sala, V. Vlachoudis, G. Smirnov, Overview of the FLUKA code, Ann. Nucl. Energy. 82 (2015) 10–18. https://doi.org/10.1016/j.anucene.2014.11.007.

[27] E. V. Pagano, M.B. Chatterjee, E. De Filippo, P. Russotto, L. Auditore, G. Cardella, E. Geraci, B. Gnoffo, C. Guazzoni, G. Lanzalone, S. De Luca, C. Maiolino, N.S. Martorana, A. Pagano, M. Papa, T. Parsani, S. Pirrone, G. Politi, F. Porto, L. Quattrocchi, F. Rizzo, A. Trifirò, M. Trimarchi, Pulse shape discrimination of plastic scintillator EJ 299-33 with radioactive sources, Nucl. Instruments Methods Phys. Res. Sect. A Accel. Spectrometers, Detect. Assoc. Equip. 889 (2018) 83–88. https://doi.org/10.1016/j.nima.2018.02.010.

[28] G. Dietze, Energy calibration of NE-213 scintillation counters by x-rays, IEEE Trans. Nucl. Sci. 26 (1979) 398–402. https://doi.org/10.1109/TNS.1979.4329665.

[29] W. Steinberger, M.L. Ruch, S.A. Pozzi, Performance of stilbene bars coupled to silicon photomultipliers using Different Reflectors, 2017 IEEE Nucl. Sci. Symp. Med. Imaging Conf. NSS/MIC 2017 - Conf. Proc. (2018) 12–14. https://doi.org/10.1109/NSSMIC.2017.8532739.

[30] M.P. Taggart, P.J. Sellin, Comparison of the pulse shape discrimination performance of plastic scintillators coupled to a SiPM, Nucl. Instruments Methods Phys. Res. Sect. A Accel. Spectrometers, Detect. Assoc. Equip. 908 (2018) 148–154. https://doi.org/10.1016/j.nima.2018.08.054.

[31] M. Grodzicka-Kobylka, T. Szczesniak, M. Moszyński, K. Brylew, L. Swiderski, J.J. Valiente-Dobón, P. Schotanus, K. Grodzicki, H. Trzaskowska, Fast neutron and gamma ray pulse shape discrimination in EJ-276 and EJ-276G plastic scintillators, J. Instrum. 15 (2020). https://doi.org/10.1088/1748-0221/15/03/P03030.

[32] F. Pozzi, R.G. Alia, M. Brugger, P. Carbonez, S. Danzeca, B. Gkotse, M.R. Jaekel, F. Ravotti, M. Silari, M. Tali, CERN irradiation facilities, Radiat. Prot. Dosimetry. 180 (2018) 120–124. https://doi.org/10.1093/RPD/NCX187.

[33] D.S. McGregor, J. Kenneth Shultis, Reporting detection efficiency for semiconductor neutron detectors: A need for a standard, Nucl. Instruments Methods Phys. Res. Sect. A Accel. Spectrometers, Detect. Assoc. Equip. 632 (2011) 167–174. https://doi.org/10.1016/j.nima.2010.12.084.

[34] N. Dinar, D. Celeste, P. Puzo, M. Silari, Characterization of CLYC scintillator coupled with photomultipliers and a large SiPM array, Radiat. Prot. Dosimetry. 180 (2018) 399–402. https://doi.org/10.1093/RPD/NCX203.

[35] E. Mullin, K. Mesick, S. Nowicki, D. Coupland, N. Zaitseva, K. Ianakiev, Performance characterization of organic pulse shape discrimination scintillators at Los Alamos National Laboratory (2018) 30517.

[36] J.H. Baker, N.Z. Galunov, O.A. Tarasenko, Variation of scintillation light yield of organic crystalline solids for different temperatures, IEEE Trans. Nucl. Sci. 55 (2008) 2736–2738. https://doi.org/10.1109/TNS.2008.2002146.

[37] P. Schuster, E. Brubaker, Investigating the anisotropic scintillation response in anthracene through neutron, gamma-ray, and muon measurements, IEEE Trans. Nucl. Sci. 63 (2016) 1942–1954. https://doi.org/10.1109/TNS.2016.2542589.

[38] A.S. Beddart, T.R. Mackie, F.H. Attix, Water-equivalent plastic scintillation detectors for high-energy beam dosimetry: I. Physical characteristics and theoretical considerations, 1992.

[39] L. Wootton, S. Beddar, Temperature dependence of BCF plastic scintillation detectors, Phys. Med. Biol. 58 (2013) 2955–2967. https://doi.org/10.1088/0031-9155/58/9/2955.

[40] L. Peralta, Temperature dependence of plastic scintillators, Nucl. Instruments Methods Phys. Res. Sect. A Accel. Spectrometers, Detect. Assoc. Equip. 883 (2018) 20–23. https://doi.org/10.1016/j.nima.2017.11.041.